Journal of Power Sources 194 (2009) 655–661

Contents lists available at ScienceDirect

Journal of Power Sources

journal homepage: www.elsevier.com/locate/jpowsour

Use of purine and pyrimidine bases as nitrogen sources of active site in oxygen reduction catalyst

Jun Maruyama[a,*], Nobutaka Fukui[b], Masayuki Kawaguchi[b], Ikuo Abe[a]

[a] Environmental Technology Research Division, Osaka Municipal Technical Research Institute, 1-6-50, Morinomiya, Joto-ku, Osaka 536-8553, Japan
[b] Graduate School of Engineering, Osaka Electro-Communication University, 18-8, Hatsu-cho, Neyagawa, Osaka 572-8530, Japan

ARTICLE INFO

Article history:
Received 16 January 2009
Received in revised form 31 March 2009
Accepted 16 June 2009
Available online 24 June 2009

Keywords:
Polymer electrolyte fuel cell
Noble-metal-free catalyst
Oxygen reduction
Purine base
Pyrimidine base

ABSTRACT

There are increasing expectations and demands for sufficiently active noble-metal-free catalysts for the electrode reactions in polymer electrolyte fuel cells. One of the most promising candidates for the cathode catalyst is a carbon material with Fe–N_x moiety embedded on the surface as the active site. We previously found that this carbon-based catalyst was formed by heat treatment of a mixture of Fe lactate, glucose, and amino acids as the nitrogen sources of the active site. In this study, various purine and pyrimidine bases were used as the nitrogen sources for the active site generation in order to obtain fundamental information on the activity enhancement of the carbon-based noble-metal-free cathode catalyst. The specific surface area and the surface Fe concentration of the carbon material formed by heat treatment of the Fe lactate–glucose–base mixture were dependent on the molecular structure and the number of nitrogen atoms contained in the molecule of the base, which then affected the catalytic activity for oxygen reduction and the number of electrons involved in the per oxygen molecule. Especially, the activity increased with an increase in the number of nitrogen atoms contained in the molecule. Efficient generation of the active site was also observed.

1. Introduction

Many studies are now reported about noble-metal-free catalysts for cathodes of polymer electrolyte fuel cells (PEFCs) [1–17]. It has been recognized that the noble-metal-free catalyst is highly important for realization of widespread use of PEFC to solve problems caused by using noble metals in the electrode, such as limitation of the resources and possible cost inflation, especially in the cathode due to necessity of the high amount of catalyst to compensate the slow reaction rate of the cathodic oxygen reduction. However, the noble-metal-free catalyst with sufficient activity and reliability for the PEFC electrode reactions to substitute the conventional Pt-based catalysts has not been developed so far.

Among various types of noble-metal-free fuel cell cathode catalysts, carbon materials with Fe ion coordinated by N atoms (Fe–N_x moiety) embedded on the surface as the active site have been most extensively studied and are one of the promising candidates for the active and reliable catalyst. Also from the aspect of the widespread use of the PEFC, the usage of Fe might be advantageous due to the abundance and inexpensiveness of Fe.

We recently formed a noble-metal-free fuel cell cathode catalyst with Fe–N_x active site by heat treatment of the mixture of Fe(II) lactate trihydrate, glycine, and glucose. Glycine, the simplest amino acid, functioned as the N source for the Fe–N_x active site and glucose, the most familiar monosaccharide, was added for obtaining carbon materials, since amino acids alone decompose below 350 °C to result in the failure of carbonization [18]. Although the activity was lower than that of the conventional Pt-based catalysts, we found that an increase in the glycine content in the starting mixture improved the activity, indicating that the amount of the Fe–N_x active site was increased with an increase in the amount of the N source. We also formed noble-metal-free cathode catalysts using glucose, Fe(II) lactate trihydrate, and amino acids containing more than one N atom in the molecule, and found that the activity of the catalyst increased with an increase in the number of N atoms in the amino acid molecule, which was attributed to the improved efficiency of the Fe–N_x active site generation [19].

The starting materials to form the noble-metal-free cathode catalysts in the methods of our previous studies are closely related to natural compounds, which are often commonplace, safe, and inexpensive. One of the main significance of these studies would be showing the possibility to form the noble-metal-free catalysts from such compounds, which are advantageous for the widespread use of the PEFCs. The possibility of N-containing natural compounds

* Corresponding author. Tel.: +81 6 6963 8043; fax: +81 6 6963 8049.
E-mail address: maruyama@omtri.city.osaka.jp (J. Maruyama).

0378-7753/$ – see front matter © 2009 Elsevier B.V. All rights reserved.
doi:10.1016/j.jpowsour.2009.06.048

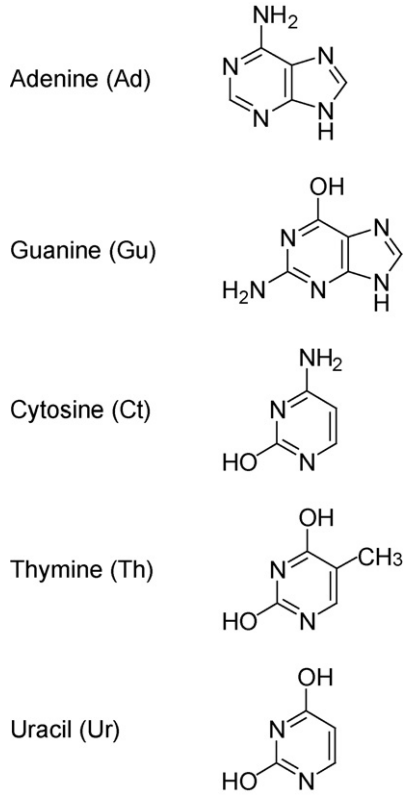

Fig. 1. Molecular structures of purine and pyrimidine bases used in this study.

other than amino acids as the starting materials in the methods was shown by our preceding study using adenine [20]. Adenine (Ad) is a constituent of nucleotides, which are also formed from, such as, guanine (Gu), cytosine (Ct), thymine (Th), uracil (Ur), the most familiar purine and pyrimidine bases (Fig. 1). These bases contain various numbers of N atoms, and one or two aromatic rings in their molecules. In our previous study [19], we used amino acids containing aromatic rings as well as those without aromatic rings; however, the influence of the molecular structure of the N sources on the behavior of the formation of the catalyst was not fully clarified. It was not clear either whether the enhancement of the catalytic activity by the increase in the number of N atoms in the molecule was possible in another series of N sources with different molecular structures. In order to obtain further fundamental information on the activity enhancement of the carbon-based noble-metal-free cathode catalyst, we investigated the influence of the kind of the N sources on the activity of the catalyst using these purine and pyrimidine bases in this study.

2. Experimental

2.1. Materials

The purine and pyrimidine bases were purchased from Wako Pure Chemical Industries. Glucose and iron(II) lactate trihydrate were purchased from Nacalai Tesque. They were used as received. High-purity water was obtained by circulating ion-exchanged water through an Easypure water-purification system (Barnstead, D7403). Perchloric acid (70%, Tama Chemicals, ultra pure analytical reagent) and sulfuric acid (98%, Tama Chemicals, ultra pure analytical reagent) were diluted with high-purity water to prepare 0.1 mol dm^{-3} $HClO_4$ and 0.5 mol dm^{-3} H_2SO_4, respectively. Solutions of Nafion as a perfluorosulfonate ion-exchange resin [equivalent weight (molar mass/mol of ion-exchange site) = 1100, 5 dissolved in a mixture of lower aliphatic alcohols and 15–20% water] were purchased from Aldrich.

2.2. Formation of the carbon material with an Fe–N_x active site

The purine and pyrimidine bases, glucose, and iron(II) lactate trihydrate were mixed and ground with a mortar until all of the powder passed a 100 mesh sieve (aperture, 150 μm). The molar ratio of the amino acid to glucose was set at 1 and the Fe content in the mixture was 1 wt%. The Fe content was set to add a sufficient amount of Fe in the mixture, based on the study by Wang et al. reporting that the activity of the Fe–N_x type catalyst was dependent on the Fe loading and reached the maximum at 0.16–2 wt % [21]. The mixture was heated at 150 °C in air for 24 h for dehydration of glucose, which is often carried out before the carbonization of glucose. After grinding this dehydrated mixture similarly, the powder was heated in 100 cm^3 min^{-1} of flowing Ar at 1000 °C for 2 h after raising the temperature at 5 °C min^{-1}. The sample was ground again until all of the powder passed through a 330 mesh sieve (aperture, 45 μm) and a treatment with an acid solution was carried out to remove soluble Fe species. The treatment was performed in 0.5 mol dm^{-3} H_2SO_4 at a boiling temperature for 1 h, followed by filtering, washing with high-purity water, and drying in vacuum at room temperature. For convenience, the sample produced using Bs (Bs = Ad, Gu, Ct, Th, Ur) is hereafter called GBsI. The samples using glycine and arginine as the nitrogen sources were produced similarly for comparison and are hereafter called GGI and GRI, respectively.

2.3. Characterization of the carbon materials

The Fe contents in the carbon materials were measured by inductively coupled plasma atomic emission spectrophotometry (ICP-AES) using an ICPS-8100 system (Shimadzu) after combustion of the carbon matrix and dissolution of the residue by 0.5 mol dm^{-3} H_2SO_4 at a boiling temperature. The adsorption isotherm of N_2 onto the carbon material was measured using an automatic N_2 adsorption apparatus (Belsorp 28, Nihon Bell) at −196 °C. The specific surface area was determined by the Brunauer–Emmet–Teller (BET) plot of the isotherm. The X-ray diffraction (XRD) was performed with an automated RINT 2500 X-ray diffractometer (Rigaku) using Cu Kα radiation. The data acquisition was carried out in the $\theta/2\theta$ step scanning mode at a speed of 1° min^{-1} with a step size of 0.02° (2θ). The X-ray photoelectron spectroscopy (XPS) was carried out using a PHI ESCA 5700 system (Physical Electronics) with Al Kα radiation (1486.6 eV), in which the finely ground carbonized material was fixed on an Al adhesive tape. The measurements of the extended X-ray absorption fine structures (EXAFS) were performed in the transmission mode in air at room temperature using synchrotron radiation at the beam lines of BL-7C of the Photon Factory in the High Energy Accelerator Research Organization and BL19B2 of SPring8 in the Japan Synchrotron Radiation Research Institute. Fourier transformation was performed on a k^3-weighted EXAFS spectrum using a REX2000 program (Rigaku) to calculate the pseudo-radial distribution function (RDF).

2.4. Catalyst layer formation

The electrochemical characteristics of the carbon material were investigated by fixing it on the surface of a rotating glassy carbon disk electrode (GC RDE) as a catalyst layer and immersing it in 0.1 mol dm^{-3} $HClO_4$ [22–24]. An aliquot of 50 mg of the carbon material and 5 mg of carbon black (Vulcan XC-72R, Cabot) as the electron-conductive agent were added to 1.0 cm^3 of a Nafion solution which was prepared by diluting 0.5 cm^3 of the 5 wt% Nafion solution with high-purity water. The mixture was ultrasonically

Table 1
Yields, Fe contents, and specific surface areas (S) of GAdI, GGuI, GCtI, GThI, and GUrI.

	Yield (%)			Fe content (wt%)	S ($m^2\,g^{-1}$)
	Heat treatment at 150 °C	Heat treatment at 1000 °C	Total		
GAdI	77.5	8.9	6.9	0.15	425
GGuI	83.1	11.5	9.6	0.30	450
GCtI	74.9	18.2	13.6	0.34	192
GThI	84.9	6.0	5.1	0.50	582
GUrI	80.9	13.4	10.8	0.12	291

dispersed to produce a catalyst paste. A GC RDE (BAS), which consisted of a GC rod sealed in a Kel-F holder, was polished with a 2000 grit emery paper (Sumitomo 3 M) and then ultrasonically cleaned in high-purity water for use as a support for the catalyst layer. The geometric surface area of the electrode was 0.071 cm^2 (diameter, 3 mm). A 1 mm^3 volume of the paste was pipetted onto the GC surface, and to shield it from the irregular air stream generated by a ventilator, the electrode was immediately placed under a glass cover until the layer was formed. This operation was repeated once again to load 100 μg of the carbon material on the GC surface. After removal of the glass cover, the layer was further dried overnight at room temperature.

2.5. Electrochemical measurements

An electrochemical analyzer (100B/W, BAS) and an RDE glass cell were used for cyclic voltammetry and measurements of the current–potential relationships. The glass cell was cleaned by soaking in a 1:1 mixture of concentrated HNO_3 and H_2SO_4, followed by a thorough rinsing with high-purity water, and finally steam cleaning [25]. The counter electrode was a Pt wire, and the reference electrode was a reversible hydrogen electrode (RHE). All potentials were referred to the RHE. Cyclic voltammograms for the catalyst layers were recorded in Ar-saturated 0.1 mol dm^{-3} $HClO_4$ at 25 °C. The potential was scanned between 0.05 and 1.3 V at a scan rate of 50 mV s^{-1}. Before recording, the potential was repeatedly scanned between 0.05 and 1.4 V to remove any residual impurities. The current–potential relationships were obtained in O_2-saturated 0.1 mol dm^{-3} $HClO_4$ at 25 °C at various rotation speeds. The scan rate of the potential was fixed at 10 mV s^{-1}. Prior to measurement, the electrode was repeatedly and alternately polarized at 0.05 and 1.3 V [26]. The potential was finally stepped to 1.2 V and then swept in the negative direction to obtain the current–potential relationship. The background current was similarly measured in an Ar atmosphere without rotation.

3. Results and discussion

3.1. Formation of carbon materials

The heat treatment of the mixture of the purine or pyrimidine bases, glucose, and Fe(II) lactate trihydrate at 150 °C in air for 24 h produced the precursor and the heat treatment of the precursor at 1000 °C in flowing Ar for 2 h produced the carbon material. The yields of the precursors and those of the carbon materials are summarized in Table 1. The total yield was calculated by multiplying the yield of the precursor by that of the corresponding carbon material from the precursor.

The yields of the precursors shown in Table 1 tended to be higher than those for the precursor obtained by the mixture of amino acids, glucose and Fe(II) lactate trihydrate in the preceding study [19], The relatively higher yields were obtained for the precursor formed using the amino acids that contained aromatic rings in the molecular structure [19]. According to this result, the higher yield obtained in this study was attributable to the molecular structure of the bases. In contrast, the yields of the carbon material formed from using the amino acids that contained aromatic ring in the molecular structure tended to be lower compared to those formed using amino acids without aromatic rings [19]. These lower yields were also in agreement with the yields of the carbon material formed using the purine or pyrimidine bases, which tended to be lower compared to those formed from amino acids without aromatic rings. Therefore, these results indicated that the yields for the precursor and the carbon materials were dependent on the molecular structure of the nitrogen sources.

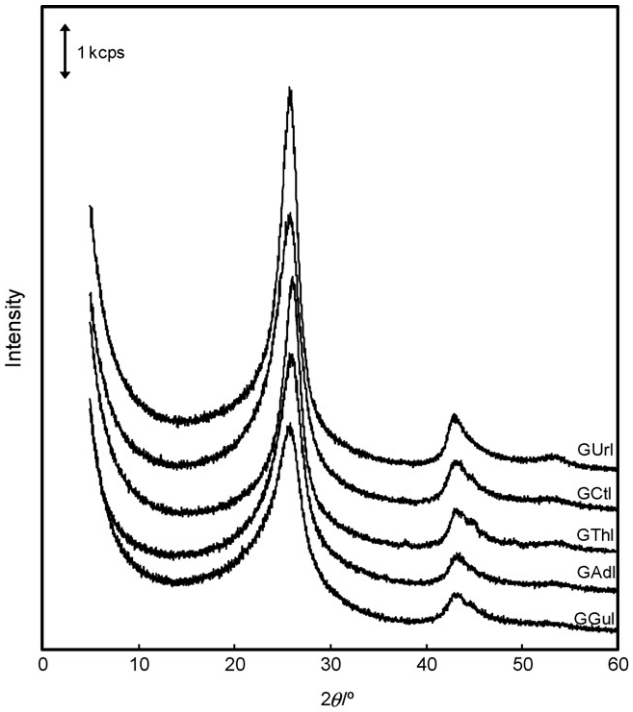

Fig. 2. X-ray diffraction spectra of GAdI, GGuI, GCtI, GThI, and GUrI. Cu-Kα radiation was used. Each spectrum is shifted by 1 kcps for easier comparison.

The specific surface area of the carbon materials (Table 1) was also dependent on the molecular structure of the purine and pyrimidine bases. The specific surface areas of the carbon materials formed using the pyrimidine bases were lower compared to those formed using the purine bases except that of GThI. The exceptional high specific surface area of GThI might be due to the molecular structure, in which three functional groups are connected to the aromatic ring. The higher specific surface area of GGuI than that of GAdI was also associated with the number of functional groups, although detailed reason is not clear at present. In the preceding study [19], the carbon material with the relatively high surface area was formed using tryptophan, which possesses two fused aromatic rings in the molecule. The higher specific surface areas of GAdI and GGuI than the carbon materials formed using the pyrimidine bases except Th might also be associated with the molecular structure.

The structural regularity of the carbon matrix was slightly dependent of the kind of the base. Fig. 2 shows the XRD spectra of the carbon materials. These spectra are typical of amorphous carbon, such as carbon black and activated carbon. The sharp (0 0 2) diffraction peak at 26°, the (1 0) peak at 43°, and the very weak (0 0 4) peak at 53° were observed for all the carbon materials. The absence of ($h\,k\,l$) diffraction peaks except the (0 0 l) peaks was attributed to a structure consisting of randomly layered graphene sheets (turbostratic structure). The intensities of these peaks were slightly higher for the carbon materials formed using the pyrimidine bases. The small peak observed for GGuI, GCtI, and GThI around

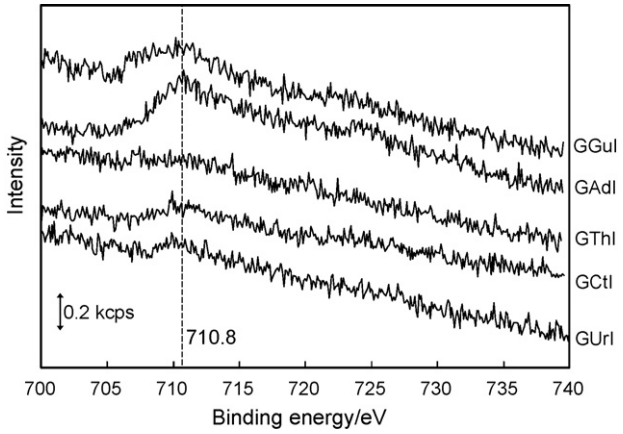

Fig. 3. X-ray photoelectron spectra of Fe 2p in GAdI, GGuI, GCtI, GThI, and GUrI. Each spectrum is arbitrarily shifted in the *y*-axis direction for easier comparison.

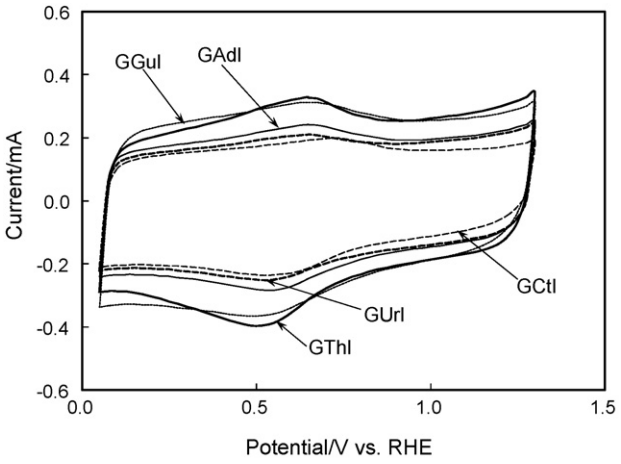

Fig. 4. Cyclic voltammograms for catalyst layers formed using GAdI (thin line), GGuI (thin dotted line), GCtI (thin dashed line), GThI (thick line), and GUrI (thick dashed line) in Ar-saturated 0.1 mol dm^{-3} $HClO_4$ at 25 °C. Scan rate: 50 mV s^{-1}.

45° was attributed to Fe(0) particles, probably included in the carbon matrix and retained after the acid treatment of the carbon material. There was also a small peak at 38° for GThI, which was attributed to Fe_3C included also in the carbon matrix. The higher Fe content in these carbon materials (Table 1) might be due to the inclusion of these Fe species.

3.2. XPS analysis

The surface of the carbon material was characterized by XPS. Fig. 3 shows the X-ray photoelectron spectra of Fe 2p in the carbon materials. The peak intensity was dependent on the kind of the base. The peaks appeared clearly in GAdI and GGuI, slightly in GCtI, but almost disappeared in GThI and GUrI. This order of the peak intensity was in agreement with the number of nitrogen atom contained in the base molecule. The peak position was nearly independent of the kind of the base. Those of the Fe $2p_{3/2}$ binding energy situated 710.8 eV, showing that the oxidation states were III, based on the peak position of the Fe $2p_{3/2}$ binding energy for Fe(III), 710.8–711.8 eV [27,28].

The ratios of elements on the surface of the carbon materials were determined by the XPS spectra of C 1s, N 1s, O 1s, and Fe 2p (Table 2), assuming that elements other than C, N, O, and Fe were negligible since the raw materials were nominally composed of these elements. Because the Fe–N_x active site might consist of Fe ion and the pyrrole-like nitrogen atoms [18], these results indicated that the increase in the number of nitrogen atom in the base molecule was efficient to expose Fe(III), although the detailed mechanism of the formation of the active site is still unclear and is necessary to be studied in the future.

3.3. Cyclic voltammetry

The surface of the carbon material in contact with the electrolyte becomes electrochemically active where electrochemical reactions occur. The information on the area was examined by cyclic voltammetry. Fig. 4 shows the cyclic voltammograms for the catalyst layer in Ar-saturated 0.1 mol dm^{-3} $HClO_4$. The sign of the current due to the oxidation reactions was taken as positive and that due to the reduction reactions was taken as negative. The current was generated by charging of the electrochemical double-layer and the redox reaction of quinone-like functional groups (Qn) on the surfaces, which is usually observed for carbon electrodes [29]:

$$Qn + 2H^+ + 2e^- \leftrightarrow QnH_2 \quad (1)$$

Theoretically, the charging current of the electrochemical double-layer is proportional to the electrochemically active surface area. The oxidation and reduction of the quinone-like functional groups were observed as the broad peaks centered at around 0.65–0.7 and 0.5–0.55 V, respectively. The currents associated with these reactions are also proportional to the electrochemically active surface area, assuming that the functional groups are homogeneously distributed on the surface. The current in the voltammogram for the catalyst layer formed from GBsI was nearly in agreement with the specific surface area of corresponding GBsI.

Table 2
Ratios of elements on the surface of GAdI, GGuI, GCtI, GThI, and GUrI (at.%).

	GAdI	GGuI	GCtI	GThI	GUrI
C	95.37	95.34	96.37	97.26	97.00
N	0.71	1.04	0.73	0.29	0.42
O	3.78	3.52	2.83	2.39	2.52
Fe	0.14	0.10	0.07	0.06	0.06

The ratios of the elements on the surface of the carbon materials were calculated assuming that those of the elements other than C, N, O, and Fe were negligible since the raw materials were nominally composed of these elements.

3.4. Oxygen reduction

Oxygen reduction currents at the catalyst layers were measured in O_2-sarturated 0.1 mol dm^{-3} $HClO_4$ with the electrodes being rotated at various rotation speeds. Fig. 5 shows the relationships between the electrode potential and the currents at the catalyst layers measured by rotating the electrodes at 2000 rpm. The current shown in Fig. 5 was obtained by subtracting the background current from the measured current. The O_2 reduction current was varied with the kind of the base used as the starting material for the catalyst.

The activity of the catalyst layer for O_2 reduction was evaluated using the reduction current free of the influence of mass transfer in the solution, I_K, determined by the equation shown below [22].

$$-\frac{1}{I} = -\frac{1}{I_K} + \frac{1}{0.620nFAD^{2/3}c\nu^{-1/6}\omega^{1/2}} \quad (2)$$

where I is the reduction current after subtracting the background current, n is the number of electrons involved in the O_2 reduction per molecule, F is the Faraday constant, A is the geometric area of the GC electrode, D is the diffusion coefficient of O_2 in the solution, c is the concentration of O_2 in the solution, ν is the kinematic viscosity of the solution, and ω is the angular frequency of the rotation. Fig. 6 shows $-1/I$ vs. $\omega^{-1/2}$ plots for the O_2 reduction at 0.1 V and n that

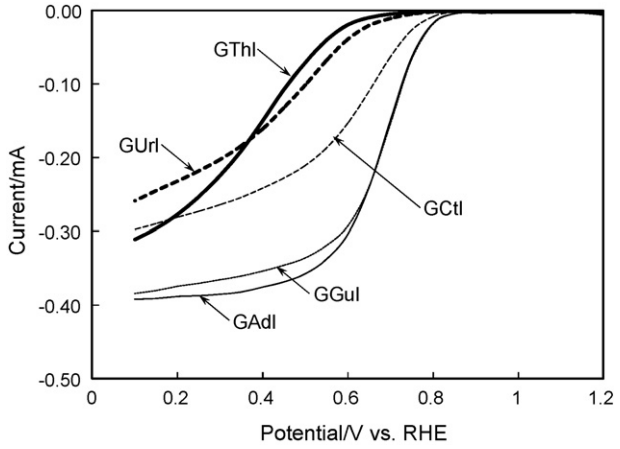

Fig. 5. Relationships between electrode potential and oxygen reduction current of negative scans at catalyst layers formed using GAdI (thin line), GGuI (thin dotted line), GCtI (thin dashed line), GThI (thick line), and GUrI (thick dashed line) in O_2-saturated 0.1 mol dm^{-3} $HClO_4$ at 25 °C. Scan rate: 10 mV s^{-1}. Electrode rotation speed: 2000 rpm.

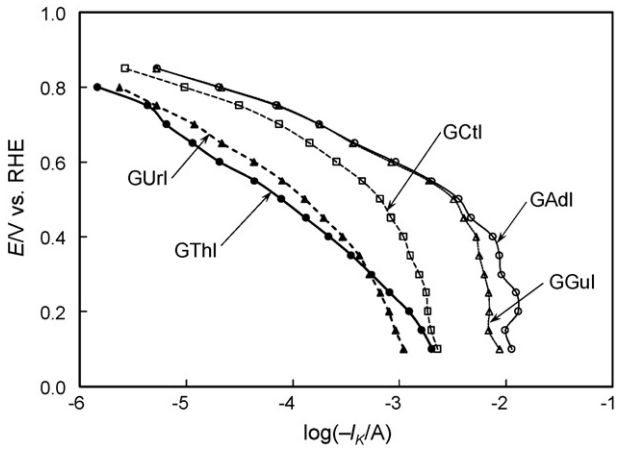

Fig. 7. Relationships between electrode potential and log($-I_K/A$) for catalyst layers formed using GAdI (○, thin line), GGuI (△, thin dotted line), GCtI (□, thin dashed line), GThI (●, thick line), and GUrI (▲, thick dashed line).

were calculated using the slope of the plot and the following values [30–32]: $F = 96485$ C mol^{-1}; $A = 0.0707$ cm^2; $D = 1.9 \times 10^{-5}$ cm^2 s^{-1}; $c = 1.18 \times 10^{-6}$ mol cm^{-3}; $\nu = 9.87 \times 10^{-3}$ cm^2 s^{-1}. The relationships between the electrode potential and log($-I_K/A$) (Tafel plots) are shown in Fig. 7.

$-I_K$ was dependent on the kind of the base and increased with an increase in the number of nitrogen atoms contained in the base. This tendency was in agreement with the increase in the ratio of Fe on the surface of the carbon material determined by XPS; therefore, the increase in $-I_K$ was attributed to the increase in the active site on the surface of the carbon materials. The highest n observed for the catalyst layers formed using GAdI and GGuI was also associated with the high surface concentration of the active site. A two-electron reduction generates the intermediate H_2O_2 (Eq. (3)). An increase in n occurs with further reduction (Eq. (4)), the decomposition of H_2O_2 (Eq. (5)), or an increase in the proportion of the four-electron reduction to H_2O (Eq. (6)) [33].

$$O_2 + 2H^+ + 2e^- \rightarrow H_2O_2 \quad (3)$$

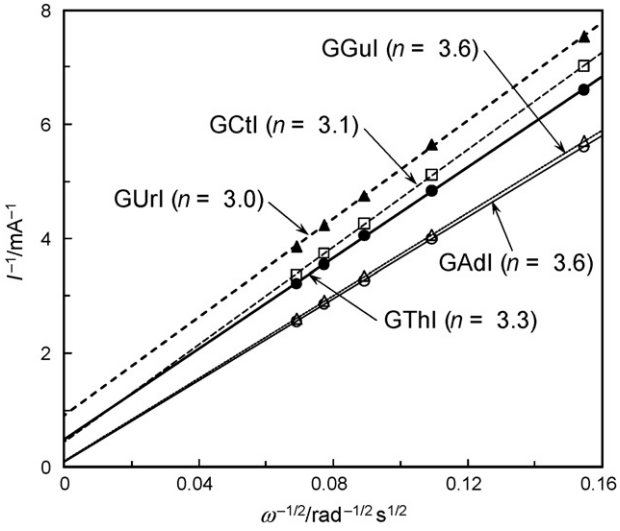

Fig. 6. $-1/I$ vs. $\omega^{-1/2}$ plots for oxygen reduction and number of electrons involved in the reaction per molecule at 0.1 V for catalyst layers formed using GAdI (○, thin line), GGuI (△, thin dotted line), GCtI (□, thin dashed line), GThI (●, thick line), and GUrI (▲, thick dashed line).

$$H_2O_2 + 2H^+ + 2e^- \rightarrow 2H_2O \quad (4)$$

$$2H_2O_2 + 2H_2O + O_2 \quad (5)$$

$$O_2 + 4H^+ + 4e^- \rightarrow 2H_2O \quad (6)$$

The n increase was caused by the increase in the active site and the development of the micropores in the catalyst, because the latter raised the possibility that H_2O_2 molecules generated inside the catalyst layer were further reduced or decomposed during their transfer to the outside of the layer, which resulted in the n increase. The n increase might be also possible by the reduction of H_2O_2 or its decomposition at the other catalyst particles inside the catalyst layer. The dependence of n on the density of the catalyst particle in the catalyst layer was suggested by Inaba et al. [34]. In this study, however, this possibility could be excluded because the catalyst layers of the five catalysts were formed in the same way. Thus, the relative comparison between the catalysts was valid. The relatively high n for the GThI layer in spite of the low ratio of Fe on the surface of GThI might be due to the developed pore structure in the catalyst particles. The higher n values for the GAdI and the GGuI layers than the GCtI and the GUrI layers were also partly attributed to the higher specific surface area of the formers.

3.5. EXAFS results

In addition to the high surface Fe concentration and the developed pore structure observed for the carbon materials formed using the purine bases, the efficient generation of the active site was indicated by the results of the EXAFS measurements at the Fe K-edge for the carbon material. Fig. 8 shows the Fe K-edge RDFs for the Fe foil, α-Fe_2O_3, γ-Fe_2O_3, hematin, Fe phthalocyanine, GGI, GRI, and GAdI, which showed the best catalytic activity among the carbon materials formed in this study based on the $-I_K$. In the RDF for hematin, the first peak at around 1.7 Å was attributed to four N atoms coordinating to the Fe(III) center. The shoulder at around 1.2 Å was attributed to OH^- coordinating perpendicular to the macrocyclic plane to the Fe center. The second peak was attributed to the C atoms, which were bound to the N atom in the pyrolic ring and the bridging C connecting the pyrolic rings. Comparing the RDF for GGI with that for hematin, the peak at 1.5 Å and the shoulder at around 3 Å observed in the RDF for GGI were attributed to the Fe–N_x active site. Although it is recognized that the identification of the nearest neighbor atom only from the EXAFS result is difficult, it might be reasonable to assume the presence of the Fe–N_x moiety in the catalysts formed using the amino acids as the N sources on the basis of the results of

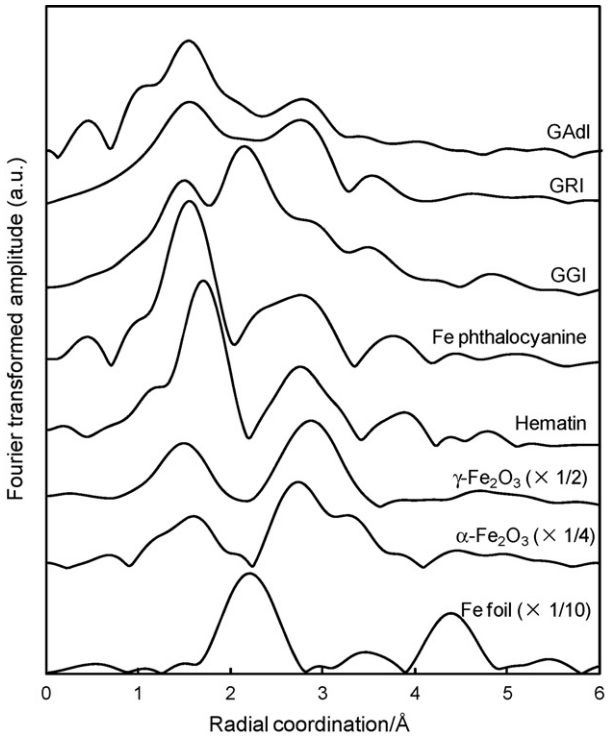

Fig. 8. Pseudo-radial distribution functions calculated by Fourier transformation of extended X-ray adsorption fine spectra at the Fe K-edge for Fe foil, α-Fe_2O_3, γ-Fe_2O_3, hematin, Fe phthalocyanine, GGI, GRI, and GAdI.

the Mössbauer spectrum of GGI shown in reference 18, which was similar to the carbonized catalase containing the Fe–N_x moiety. The first peak position negatively shifted, suggesting that the distance between Fe and N was shorter than that in hematin and became close to that of Fe phthalocyanine. The largest peak at 2.2 Å in the RDF was attributed to the Fe(0) included in the carbon matrix of GGI, comparing the RDF to that for the Fe foil. The peak attributed to the Fe(0) disappeared in the RDF for GRI, indicating that the Fe–N_x active site was generated efficiently without generating the Fe(0), although the peak at 2.8 Å was partly attributed to the α-Fe_2O_3 and γ-Fe_2O_3 included in the carbon matrix according to the XRD result [19]. The RDF for the iron oxides shows the peak at 1.5 Å, at which the peak attributed to the Fe–N_x active site also appeared. However, the peak at the RDF for the iron oxides shows the higher peak at 2.8 Å in contrast to the RDF for hematin, GRI, and GAdI, in which the peak at 1.5 Å was higher than that at 2.8 Å. Therefore, the presence of species other than the iron oxides, the Fe–N_x active site in this case, was necessary to interpret the RDF for the carbon materials. The similarity of the RDF of GAdI to that of GRI indicated that the Fe–N_x active site was also generated in GAdI. The amplitude decrease around 2.8 Å in the RDF for GAdI also suggested that the formation of these iron oxides could be almost avoided and thus the active site was further efficiently generated using adenine as the nitrogen source.

4. Conclusions

The carbon materials with the Fe–N_x moiety embedded on the surface as the active site for oxygen reduction were formed using glucose, iron lactate, and purine and pyrimidine bases. The familiar purine and pyrimidine bases, adenine, guanine, cytosine, thymine, and uracil, were used as the nitrogen sources for the active site generation in this study. The precursor was once formed by dehydration of the mixture of the starting materials before the formation of the carbon materials. The mass loss in the formation of the precursors and the carbon material, the specific surface area of the carbon material, and the surface Fe concentration of the carbon material were dependent on the molecular structure of the bases and the number of nitrogen atoms contained in the molecule. Especially, the surface Fe concentration as well as the catalytic activity of the carbon material for oxygen reduction increased with an increase in the number of nitrogen atoms in the base molecule. The number of electrons per oxygen molecule was influenced by the pore development. Therefore, the electrochemical behavior of oxygen reduction on the carbon material was dependent on the molecular structure of the bases and the increase in the number of nitrogen atoms in the base molecule was effective for the enhancement of the catalytic activity. The activity enhancement in the catalysts in this study by the increase in the number of nitrogen atoms was common to the catalysts formed using amino acids in the previous study [19], which are the different series of nitrogen-containing natural compounds. The EXAFS results supported the efficiency of the generation of the active site. Thus useful fundamental information for the enhancement of the activity of noble-metal-free cathode catalyst was obtained using the purine and pyrimidine bases with various kinds of molecular structure and number of nitrogen atoms contained in the molecule.

Acknowledgments

We thank Mr. H. Kawano for his help with the ICP-AES measurements, and Dr. T. Shinagawa for providing the EXAFS data of Fe_2O_3. The XAFS measurements were performed with the approval of the Photon Factory (Proposal No. 2005G210) and SPring8 (Proposal nos. 2003A0863-RI-np and 2007A1470). We thank Dr. Y. Uchimoto, Mr. J. Okamura and the SPring8 members for their kind support of the measurements and the analysis. This study was partly supported by a Grant-in-Aid for Scientific Research (project no. 18750183) given to J.M. from the Ministry of Education, Culture, Sports, Science and Technology, Japan, for which the authors are grateful.

References

[1] Y. Feng, T. He, N. Alonso-Vante, Chem. Mater. 20 (2008) 26–28.
[2] F. Charreteur, F. Jaouen, S. Ruggeri, J.-P. Dodelet, Electrochim. Acta 53 (2008) 2925–2938.
[3] A. Garsuch, R. d'Eon, T. Dahn, O. Klepel, R.R. Garsuch, J.R. Dahn, J. Electrochem. Soc. 155 (2008) B236–B243.
[4] A. Ishihara, Y. Shibata, S. Mitsushima, K. Ota, J. Electrochem. Soc. 155 (2008) B400–B406.
[5] E. Proietti, S. Ruggeri, J.-P. Dodelet, J. Electrochem. Soc. 155 (2008) B340–B348.
[6] T.E. Wood, Z. Tan, A.K. Schmoekel, D. O'Neill, R. Atanasoski, J. Power Sources 178 (2008) 510–516.
[7] A.H.C. Sirk, S.A. Campbell, V.I. Birss, J. Electrochem. Soc. 155 (2008) B592–B601.
[8] J.M. Ziegelbauer, T.S. Olson, S. Pylypenko, F. Alamgir, C. Jaye, P. Atanassov, S. Mukerjee, J. Phys. Chem. C 112 (2008) 8839–8849.
[9] K. Artyushkova, S. Pylypenko, T.S. Olson, J.E. Fulghum, P. Atanassov, Langmuir 24 (2008) 9082–9088.
[10] A. Garsuch, K. MacIntyre, X. Michaud, D.A. Stevens, J.R. Dahn, J. Electrochem. Soc. 155 (2008) B953–B957.
[11] T.S. Olson, K. Chapman, P. Atanassov, J. Power Sources 183 (2008) 557–563.
[12] T. Ikeda, M. Boero, S.F. Huang, K. Terakura, M. Oshima, J.-I. Ozaki, J. Phys. Chem. C 112 (2008) 14706–14709.
[13] F. Charreteur, S. Ruggeri, F. Jaouen, J.-P. Dodelet, Electrochim. Acta 53 (2008) 6881–6889.
[14] U.I. Koslowski, I. Abs-Wurmbach, S. Fiechter, P. Bogdanoff, J. Phys. Chem. C 112 (2008) 15356–15366.
[15] M. Lefèvre, J.-P. Dodelet, Electrochim. Acta 53 (2008) 8269–8276.
[16] N. Yoshinaga, W. Sugimoto, Y. Takasu, Electrochim. Acta 54 (2008) 566–573.
[17] J. Maruyama, J. Okamura, K. Miyazaki, I. Abe, J. Phys. Chem. C 112 (2008) 2784–2790.
[18] J. Maruyama, I. Abe, J. Electrochem. Soc. 154 (2007) B297–B304.
[19] J. Maruyamaa, N. Fukui, M. Kawaguchi, I. Abe, J. Power Sources 182 (2008) 489–495.
[20] J. Maruyama, I. Abe, Chem. Commun. (2007) 2879–2881.
[21] H. Wang, R. Côté, G. Faubert, D. Guay, J.P. Dodelet, J. Phys. Chem. B 103 (1999) 2042–2049.
[22] J. Maruyama, I. Abe, Electrochim. Acta 48 (2003) 1443–1450.

[23] F. Gloaguen, F. Andolfatto, R. Durand, P. Ozil, J. Appl. Electrochem. 24 (1994) 863–869.
[24] S.Lj. Gojković, S.K. Zečević, R.F. Savinell, J. Electrochem. Soc. 145 (1998) 3713–3720.
[25] D. Chu, D. Tryk, D. Gervasio, E.B. Yeager, J. Electroanal. Chem. 272 (1989) 277–284.
[26] M. Razaq, A. Razaq, E. Yeager, D.D. DesMarteau, S. Singh, J. Electrochem. Soc. 136 (1989) 385–390.
[27] L.Y. Johansson, R. Larsson, Chem. Phys. Lett. 24 (1974) 508–513.
[28] T. Choudhury, S.O. Saied, J.L. Sullivan, A.M. Abbot, J. Phys. D: Appl. Phys. 22 (1989) 1185–1195.
[29] J. Maruyama, I. Abe, Electrochim. Acta 46 (2001) 3381–3386.
[30] J. Maruyama, I. Abe, J. Electroanal. Chem. 545 (2003) 109–115.
[31] S.K. Zečević, J.S. Wainright, M.H. Litt, S.Lj. Gojković, R.F. Savinell, J. Electrochem. Soc. 144 (1997) 2973–2982.
[32] R.M.Q. Mello, E.A. Ticianelli, Electrochim. Acta 42 (1997) 1031–1039.
[33] J. Maruyama, M. Inaba, T. Morita, Z. Ogumi, J. Electroanal. Chem. 504 (2001) 208–216.
[34] M. Inaba, H. Yamada, J. Tokunaga, A. Tasaka, Electrochem. Solid-State Lett. 7 (2004) A474–A476.